Laboratory tests and numerical modelling in the development of WaveCat

Allen, J

Proceedings of the Twelfth European Wave and Tidal Energy Conference

Laboratory Tests and Numerical Modelling in the Development of WaveCat

James Allen[#1], Konstantinos Sampanis[#2], Jian Wan[#3], Jon Miles[#4], Deborah Greaves[#5] and Gregorio Iglesias[#6]

[#]*School of Engineering, Plymouth University*
Drake Circus, Plymouth, PL4 8AA, United Kingdom

[1]james.allen@plymouth.ac.uk

[2]sabanisk@hotmail.com

[3]jian.wan @plymouth.ac.uk

[4]J.R.Miles@plymouth.ac.uk

[5]deborah.greaves@plymouth.ac.uk

[6]gregorio.iglesias@plymouth.ac.uk

Abstract— **WaveCat, a novel Wave Energy Converter, was tested with the aim of validating a numerical model based on its motion in regular waves and to provide an environment on which to determine potential power production under regular waves and irregular sea states. Tests were carried out at 1:30 scale in the Ocean Basin of the COAST Laboratory in the University of Plymouth and device motions recorded. A numerical model was designed in STAR-CCM+ and results validated with the experimental results. The results show the numerical model capable of predicting the device heave with small over prediction and the pitch with small under prediction. The numerical model will form the basis of a more complex numerical model capable of modelling the potential power output of the device under regular waves and irregular sea states with objectives toward this outlined.**

Keywords— **Wave energy converter, STAR-CCM+, physical modelling, numerical modelling, marine renewable energy**

I. INTRODUCTION

In order to reduce the impact of fossil fuels on our climate, the contribution of renewable energy to energy production must be enhanced. Within the European Union, targets have been set for member countries to produce a percentage of their energy from renewable sources [1]; for example, the UK must produce 15% of its energy share from renewable sources by 2020. In order to reach the targets set by the EU, alternative energy generation methods must be explored.

Marine renewable energy is a relatively underutilised area of energy extraction, with avenues in offshore wind, tidal stream, tidal range and wave energy available. Worldwide, wave energy potential is estimated to be 17 TW h/year [2] with the largest concentrations at mid-latitudes, 30° to 60°, which Europe is in a prime position to exploit.

For the potential of wave energy to be fully realised and commercially viable, several fundamental steps must be completed. Firstly, the resource must be assessed at each proposed site, as it can present significant spatial and temporal variation in a local area [3-6]. The uncertainty of the resource as well as the potential for weather windows allowing access to the device for operation and maintenance tasks should also be considered [7, 8]. Secondly, the impact on the local marine environment must be assessed in terms of the effect on the coastline [9-11] and the immediate marine ecosystem [12], amongst others. The above impacts are not necessarily negative, as a wave farm extracting energy from an incoming wave field can protect vulnerable coastlines [13] or other renewable energy installations [14]. Finally, a WEC must be chosen to suit the conditions in which energy extraction is occurring, both to minimise negative impacts and to efficiently capture energy in a commercially viable manner.

Numerical models are increasingly used to mitigate the need for comprehensive, often expensive, physical modelling during the development of WEC. Multiple commercial and open source packages are available, ranging from potential flow solvers, e.g. WAMIT [15], to full Computational Fluid Dynamics (CFD) suites, e.g., ANSYS [16] and OpenFOAM [17]. Validation of the numerical model must be performed prior to trusting results, therefore numerical modelling is never completely independent of physical experiments [18].

This article focuses on the WaveCat WEC and continues from previous proof of concept work [19-21] and experimental tests [22]. The article examines the motion of the WaveCat under the influence of regular waves during experimental tests. It also details the development of a numerical model of the WaveCat with regular waves tested during the experimental campaign, and further details the steps the project will take towards validating the numerical model for regular and irregular sea states. The unsteady Reynolds-averaged Navier-Stokes (RANS) based CFD package STAR-CCM+ was used. STAR-CCM+ has been used for the modelling of vessel motion at sea [23, 24]; loads experienced by vessels at sea [25]; and other types of WECs, for example, a heave type WEC [26] and an Oscillating Water Column WEC [27]. In addition, stationary breakwaters have been modelled in STAR-CCM+ [28] and other CFD packages [29], similar in operation to the WaveCat device tested in this article.

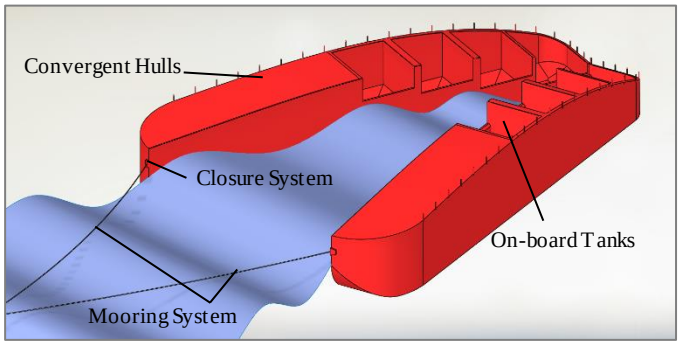

Fig. 1 The WaveCat WEC concept design

The WaveCat, Fig. 1, consists of two symmetrical hulls joined at the stern via a hinge, allowing the relative angle between the hulls to be varied depending on the sea state. In addition, the freeboard of the device decreases along the inner edge towards the stern allowing incoming waves to continue overtopping despite the reduction in height caused by the overtopping itself. Furthermore, the draft and trim of the device can be altered through the use of ballast tanks to adapt to sea states and tune the freeboard to spread overtopping volumes throughout the device. Volumes of overtopping water are collected in on-board tanks contained within the hulls and released through low-head turbines to generate electricity. The overall length of the planned prototype is 90 m and is intended to operate in water depths of between 50 m and 100 m. Typically these water depths are found further offshore, where the low profile of the device will limit visual impacts compared to large offshore structures such as wind turbines.

The device is moored via a single point to the seabed, using a Catenary Anchor Leg Mooring (CALM). This allows the device to orient itself along the direction of wave propagation passively, reducing the need for complex systems devoted to maintaining device direction. The survivability of the device is closely linked to the wedge angle. By reducing the angle to 0°, effectively closing the wedge, the device acts as a single hull body.

II. Experimental Tests

Following the initial concept tests of a 1:30 model [19-21] a new version of the WaveCat model was built at the University of Plymouth at the same scale, Fig. 2, for extended tests.

The University of Plymouth Ocean Basin was used for these experiments. The basin is 35 m in length, 15.5 m wide and 3 m deep at its maximum. The tank has a moveable floor which covered the experimental area and was set to a depth of 2 m, representing 60 m at prototype scale. The tank has 24 individually controlled, flap-type paddles to generate waves with active reflection absorption built in. There is also a parabolic beach at the down-wave end of the tank to minimise reflections.

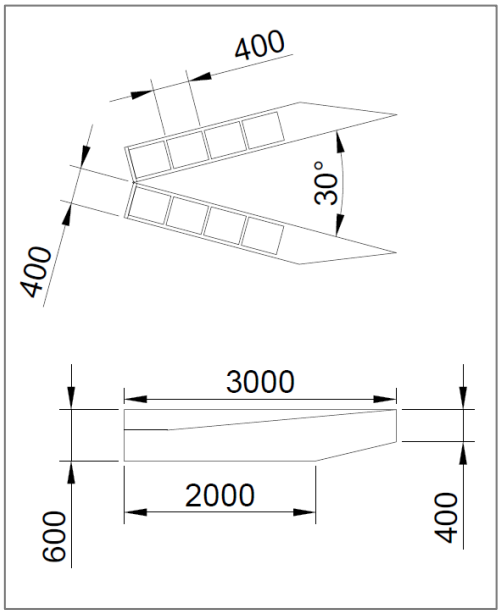

Fig. 2 The new WaveCat model plan and lateral view. Dimension in mm and at model scale, 1:30

The main dimensions of the model are length 3.0 m, height of 0.6 m and maximum width of 0.4 m. The rear 1.8 m of the model contains the tanks and the front 1.2 m is covered by the wave deflector to guide overtopping water back into the tanks.

The main body of the model was manufactured using aluminium sheet over an aluminium frame, with overtopping tanks and top mounted wave deflector constructed of polypropylene sheet. The on-board tanks were designed to be removable allowing access to the devices inner workings and ballast.

Fig 3 shows the model at a 30° wedge angle. When fully ballasted the models displacement was 520 kg, and was balanced to ensure the inner edge was parallel to the water surface, with a freeboard of 200 mm.

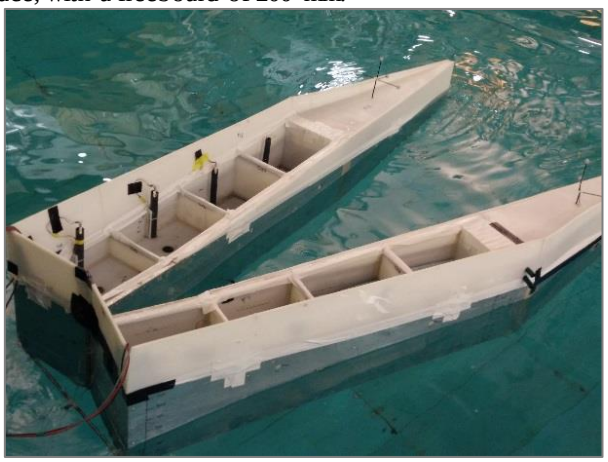

Fig. 3 The new model constructed at 1:30 scale in the University of Plymouth shown at a 30° wedge angle

The model contains resistance level sensors within each of the on-board tanks, mounted within an open pipe to reduce sloshing. Additionally, a paddle wheel flow meter was mounted

in the outlet pipe of each hull to give a combined flow reading across all four tanks. The combination of level readings and flow allowed for power generation to be estimated [22]. A microcontroller (Arduino Leonardo revision 3) was used to automatically control the release of collected water during tests when a designated level was reached in each individual tank.

A motion capture system was also used in the tests. A total of fourteen reflective markers were placed on the model, Fig. 4, which were tracked using six infrared cameras station around the wave tank. The software governing the motion capture detects the markers on the model, creates a rigid body representation and tracks the translations and rotations of the device during testing in six degrees of freedom (6DOF). The device was modelled as two fixed bodies, one representing each hull and the origin of the coordinate system located on the hinge of the device.

The device was moored using a CALM system and located approximately 17.25 m from the wave paddles, as seen in Fig. 5. A group of three resistance wave gauges (WG), WG1, WG2 and WG3, was situated before the model, along with a single gauge, WG4, at the same distance as the model to the paddles and a final group of nine gauges, WG5 to WG13 in the lee of the device. Additionally, three video cameras were mounted around the model, one of which underwater on the floor of the tank, to record video of the tests. The device was set to a wedge angle of 30° for the purposes of these experiments. 9 regular wave tests with zero angle spread were tested with characteristics described in Table I. A set of 100 waves were generated for each test and the motion of the device recorded through the Qualisys system.

Fig. 4 Showing the reflective markers on the model and the infrared Qualisys cameras mounted on tripods in the background

TABLE I
REGULAR WAVES TESTED SHOWING MODEL AND PROTOTYPE SCALE PROPERTIES

Test Case	H_m (m)	H (m)	T_m (s)	T (s)
1	0.050	1.5	1.826	10
2	0.050	1.5	2.556	14
3	0.083	2.5	1.461	8
4	0.083	2.5	2.008	11
5	0.117	3.5	1.643	9
6	0.117	3.5	1.826	10
7	0.117	3.5	2.191	12
8	0.150	4.5	1.461	8
9	0.150	4.5	2.008	11

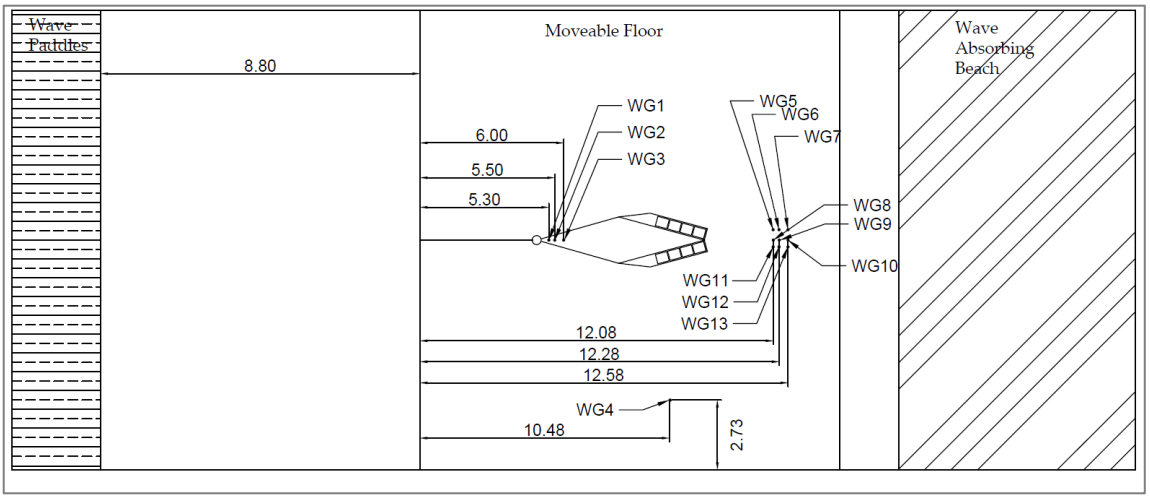

(a)

(b)

Fig. 5 Showing (a) the plan view of the experimental setup; and (b) the lateral view of the experimental setup. Dimensions in m (not to scale)

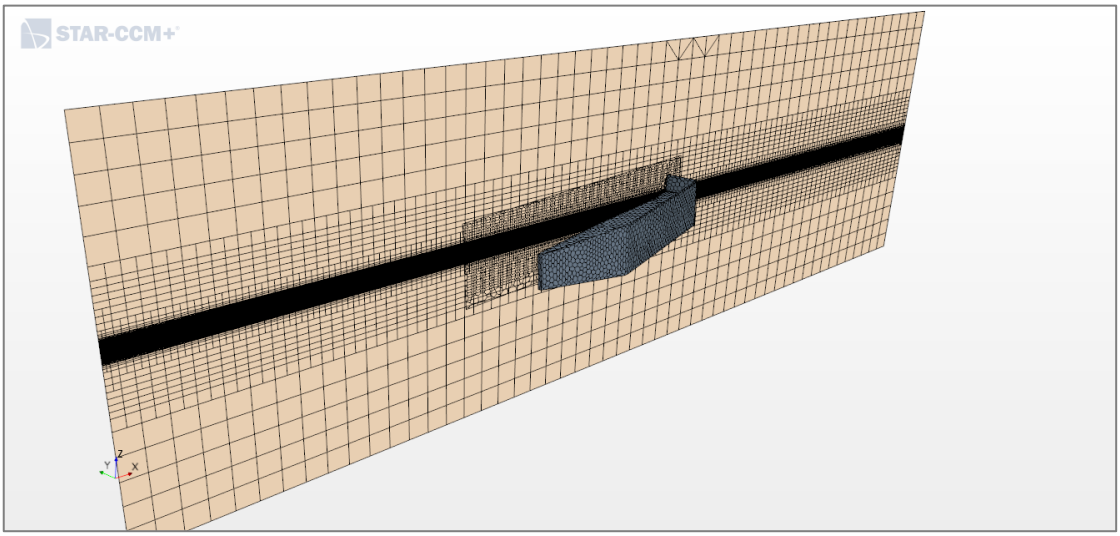

Fig. 6 Showing a plane section of the computational domain with the refined sections around the free surface and the WaveCat model in place, with the domain origin at the meeting point of the two WaveCat hulls

The experimental tests are covered in detail in another article [22], however additional tests were run for the purpose of the numerical validation. The main differences between the tests presented elsewhere and the validation tests were that the validation tests did not include overtopping of the device by means of covering the tanks. This simplifies the numerical model to not include any water oscillations present in the tank or the pipes contained within the model. Future numerical models will include this aspect of the device and the associated power generation.

III. Numerical Model

The numerical model was designed in SolidWorks and simulated in STAR-CCM+ under the effect of regular waves monitoring motion of the device

The unsteady incompressible flow was described by the continuity equation,

$$\nabla.\left[\rho\left(\bar{\mathbf{v}}-\mathbf{v}_g\right)\right]=0 \qquad (1)$$

and

$$\frac{\partial}{\partial t}(\rho\bar{\mathbf{v}})+\nabla.\left[\rho\bar{\mathbf{v}}\left(\bar{\mathbf{v}}-\mathbf{v}_g\right)\right]=-\nabla\bar{p}+\mathbf{F}_b+\nabla.\mathbf{T} \qquad (2)$$

where ρ is the density, $\bar{\mathbf{v}}$ and p are the mean velocity and pressure respectively, $\mathbf{v}_g$ is the reference frame velocity relative to the laboratory frame, $\mathbf{T}$ is the stress tensor and $\mathbf{F}_b$ is the resultant of body forces (e.g., gravity). A k-ε turbulence model and second order time step scheme were applied. The all y^+ wall treatment was also applied to the domain, which is a hybrid treatment suitable for both high and low y+ numbers and delivers the appropriate Reynolds number for each situation [30]

The computational domain was made 15 m long, 8 m wide and 4 m in height with the water depth set to 2 m to match experiments, using cubic cells with edge length of 0.25 m. The region close to the free surface was further refined to a cell size of 0.1 m and a finer refinement made to reduce the cell size further to 0.03 m in the direction of wave propagation and 0.002 m in the vertical direction.

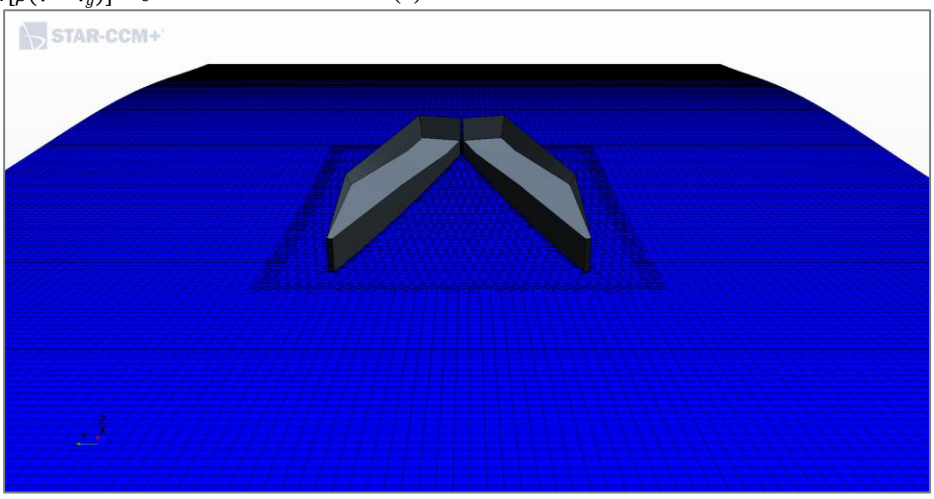

Fig. 7 Showing the free surface of the VOF wave during simulation. The overset mesh can be observed around the WaveCat device, where the cells change from cubic to polyhedral

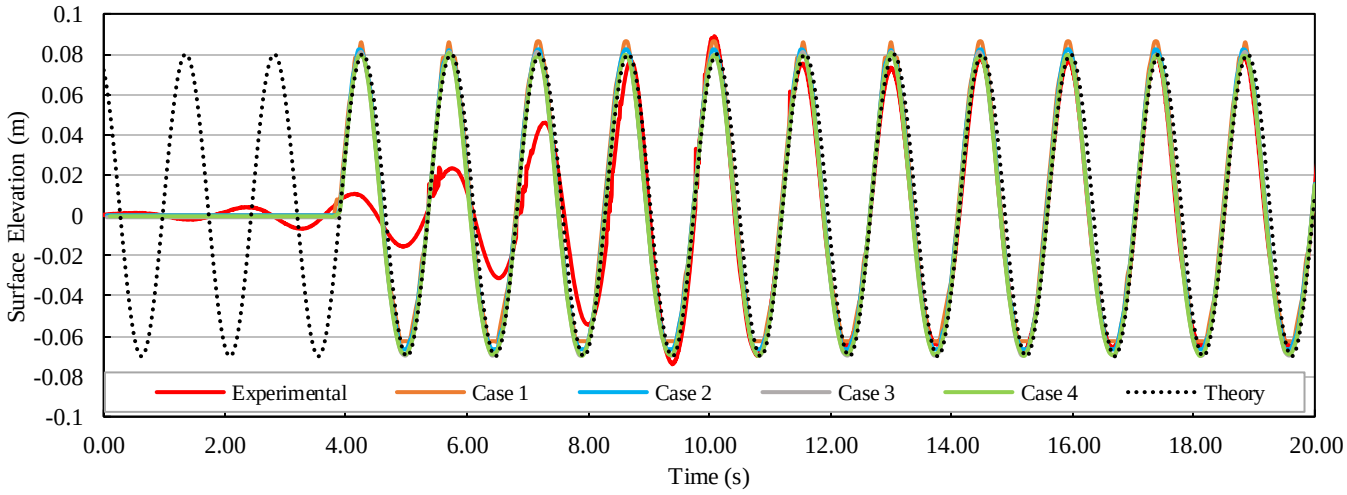

Fig. 8 Showing the mesh convergence results compared to the experimental and theoretical waves. Case 3 was chosen as a balance between reproduction of the regular wave and computational time.

The WaveCat device was modelled without the tanks in place to simplify the model mesh and reduce simulation times, similarly, during experiments with regular waves the tanks were covered. The area around the WaveCat model was refined using an overset mesh. An overset mesh captures data from a background region, in this case the larger computational domain, and transfers it to the active domain, the area around, and including, the WaveCat. The active region was modelled with polyhedral cells of the same base size at the boundary to facilitate the data transfer between the overset and background regions [31]. The WaveCat model was meshed with a polyhedral mesh with a prism layer around the exterior surface and volume refinement around the model.

The numerical model was setup to use Volume of Fluid (VOF) waves [32], generating the waves described in Table I, and control the free surface, shown in Fig. 7. The model was designated a 6DOF rigid body and allowed to rotate freely about the y-axis, pitch, and move along the z-axis, heave. The model mass was set to 520 kg and the centre of mass at (1.2, 0, 0.125) m, m, m, from an origin at the base of the hinge joint on the model, with the x-axis aligned along the axis of symmetry from stern to bow. This allows the numerical model to resolve force components on the WaveCat from the incoming VOF waves and determine the device movements.

The first stage of a numerical study is to perform mesh convergence on the proposed model to ensure the simulation is generating comparable conditions to the experimental tests. The purpose of the grid convergence study is to refine the mesh within the numerical model until further refinement produces results of the same accuracy, at which point the simulation can be considered mesh independent. As the mesh size becomes more accurate the simulation requires greater computational resources to run, thus a balance between accuracy and efficiency must be reached.

Four different mesh resolutions were tested and compared to the theoretical wave and wave produced during the experiments of the same characteristics. The mesh around the free surface was refined to varying degrees, shown in Table II. Fig. 8 shows the results of the mesh convergence tests in relation to surface elevation. From these results mesh condition 3 was chosen as a balance between accurately modelling the waves and keeping the run time realistic. The time step was to allow 240 steps per wavelength as suggested in the STAR-CCM+ user manual [30]

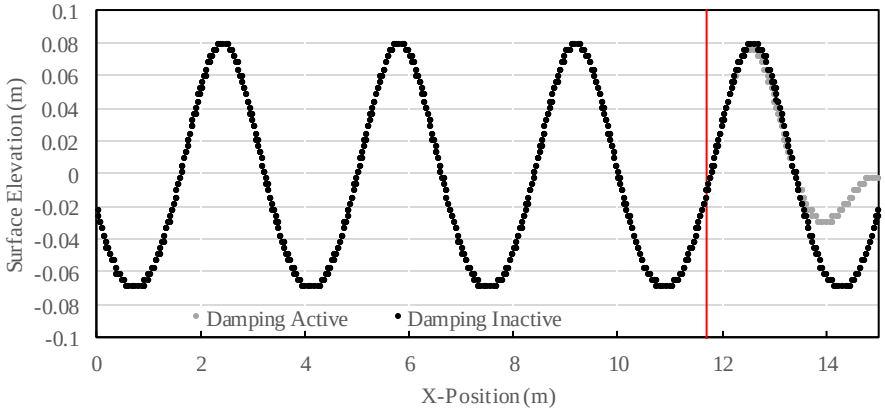

Fig. 9 Showing the effect damping has on the wave field. The red line shows the location where the damping zone begins

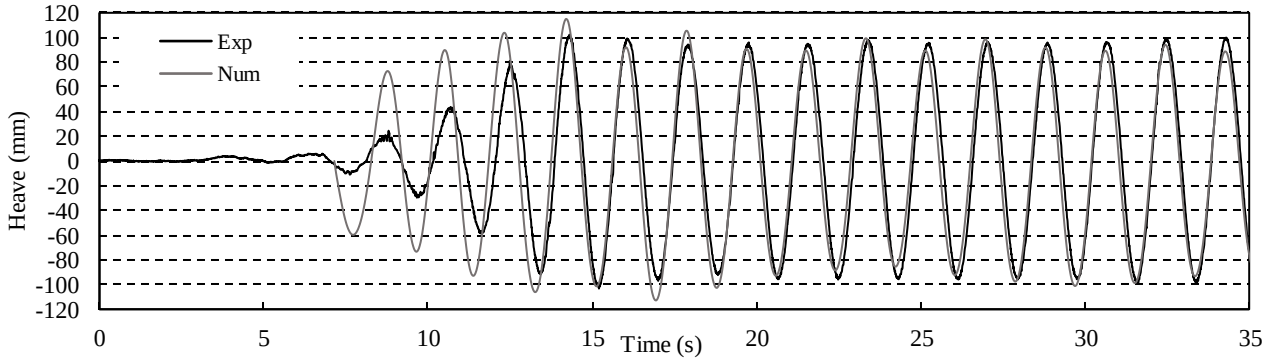

Fig. 10 Showing the full experimental and numerical heave results from test case 6, including the initial propagation from still water. The numerical data starts from a later time as the wave is initialised close to the model

TABLE II
CONVERGENCE CASES FOR THE NUMERICAL MODEL

Case	Cell height (m)	Cell length (m)	Cells per wave height	Cells per wavelength	Run time (s)
1	0.008	0.125	18	26	5,500
2	0.004	0.062	36	52	25,000
3	0.002	0.031	72	104	69,000
4	0.001	0.015	144	208	530,000

A damping zone one wavelength in length at the outlet of the domain was used to limit reflection returning to the experimental zone [33], similar to the absorbing beach present in the physical test basin. Fig. 9 shows the effect the damping zone has on the wave field.

IV. RESULTS

Test conditions outlined in Table I were simulated and device motion in y-rotation, pitch, and z-translation, heave, measured. For clarity, a section of 10 s of waves are shown from each test after the wave field has propagated to the device. Fig. 8 shows a full test including the initial wave propagation to the device. The waves propagate from nearer the device in the numerical model, hence the different start times.

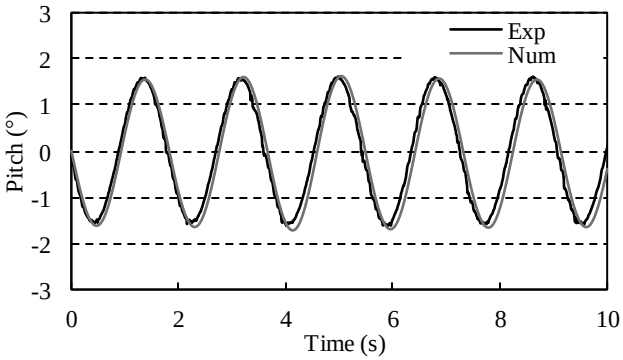

(a)

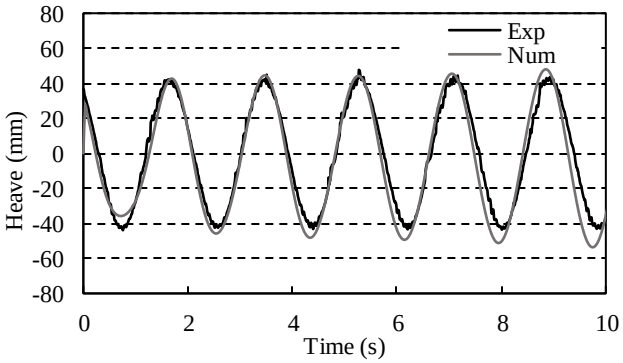

(b)

Fig. 11 (a) Pitch measurements for experimental (black) and numerical (grey); and, (b) heave measurements for experimental (black) and numerical (grey) results for test case 1

The results are also offset to provide direct comparison owing to differing coordinate systems present in the numerical and experimental tests. Heave and pitch are therefore relative values rather than absolute.

Fig. 11 shows the results of test case 1. The heave of the device is marginally over predicted in the numerical case whereas the pitch is modelled accurately.

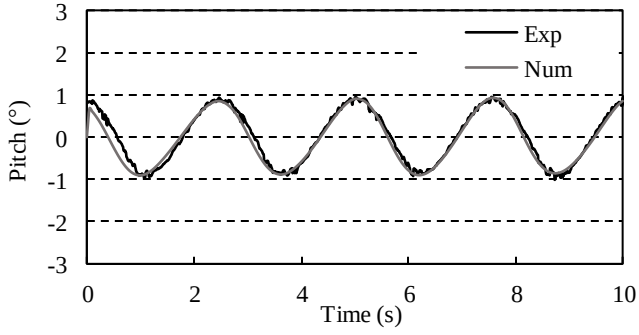

(a)

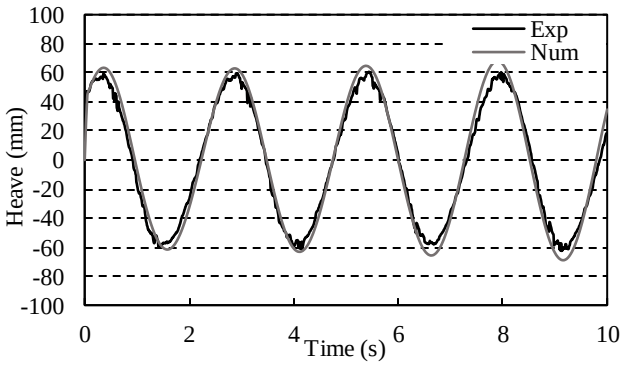

(b)

Fig. 12 (a) Pitch measurements for experimental (black) and numerical (grey); and, (b) heave measurements for experimental (black) and numerical (grey) results for test case 2

Fig. 12 shows the results of test case 2. The heave of the device is again marginally over predicted and the pitch matches the experimental results once the device is setup in the regular wave field.

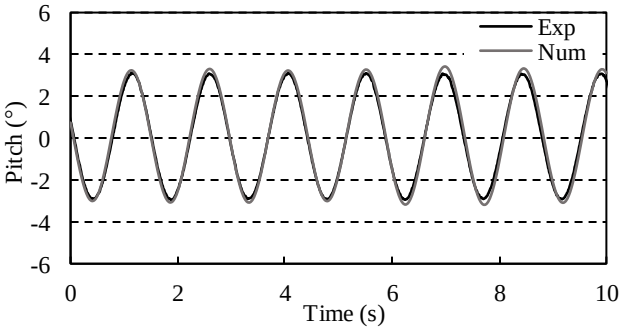

(a)

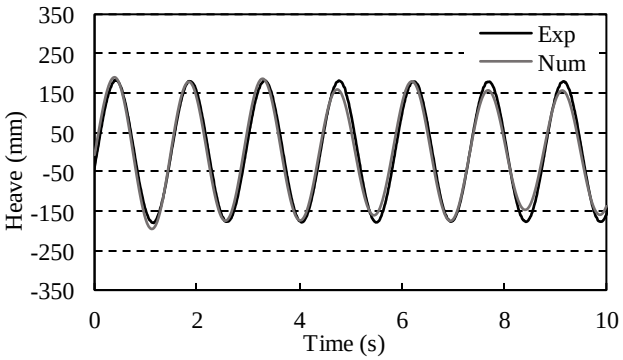

(b)

Fig. 13 (a) Pitch measurements for experimental (black) and numerical (grey); and, (b) heave measurements for experimental (black) and numerical (grey) results for test case 3

Fig. 13 shows the results of test case 3. The pitch is over predicted in the numerical model and the heave is under predicted.

Fig. 14 shows the results of test case 4. The pitch is initially over predicted in the numerical model but matches in the latter part of the run. The heave is under predicted throughout the test.

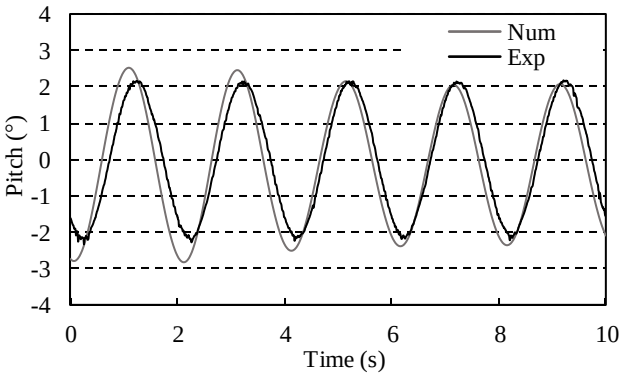

(a)

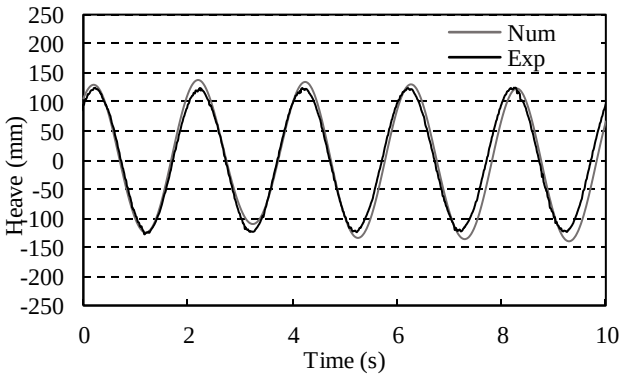

(b)

Fig. 14 (a) Pitch measurements for experimental (black) and numerical (grey); and, (b) heave measurements for experimental (black) and numerical (grey) results for test case 4

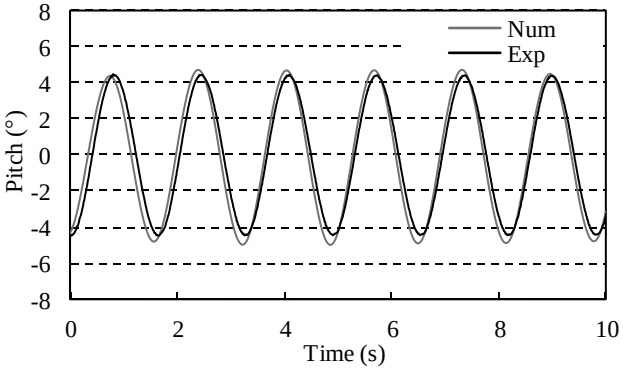

(a)

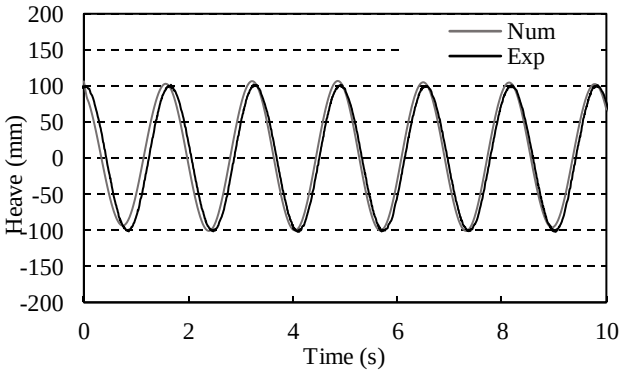

(b)

Figure 15 (a) Pitch measurements for experimental (black) and numerical (grey); and, (b) heave measurements for experimental (black) and numerical (grey) results for test case 5

Fig. 15 shows the results of test case 5. The heave is accurately modelled in the numerical model with slight variation in the period compared to the experimental data. The pitch is over predicted slightly throughout the test.

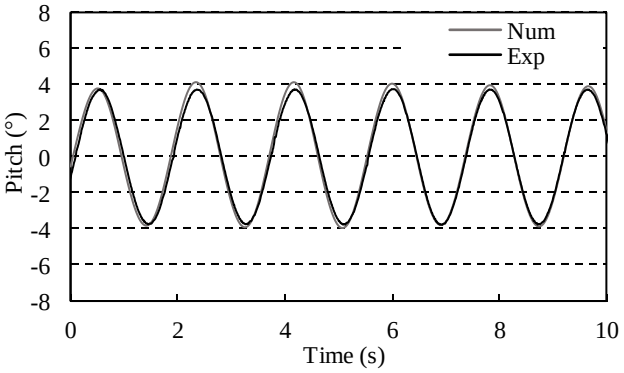

(a)

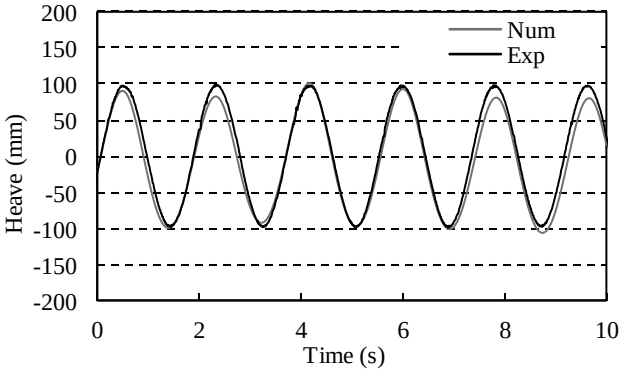

(b)

Figure 16 (a) Pitch measurements for experimental (black) and numerical (grey); and, (b) heave measurements for experimental (black) and numerical (grey) results for test case 6

Fig. 16 shows the results of test case 6. The pitch is slightly over predicted during the numerical simulation and the heave is under predicted at the maximum limits of the test.

Fig. 17 shows the results of test case 7. The pitch is over predicted as the test progresses and there is slight variation in the period of the oscillations. The heave is also slightly over predicted but agrees with the periodic oscillation.

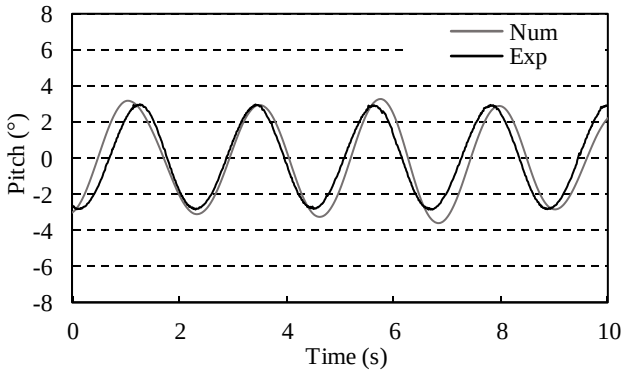

(a)

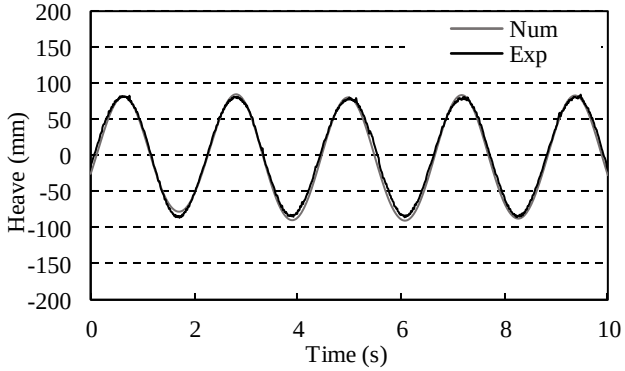

(b)

Figure 17 (a) Pitch measurements for experimental (black) and numerical (grey); and, (b) heave measurements for experimental (black) and numerical (grey) results for test case 7

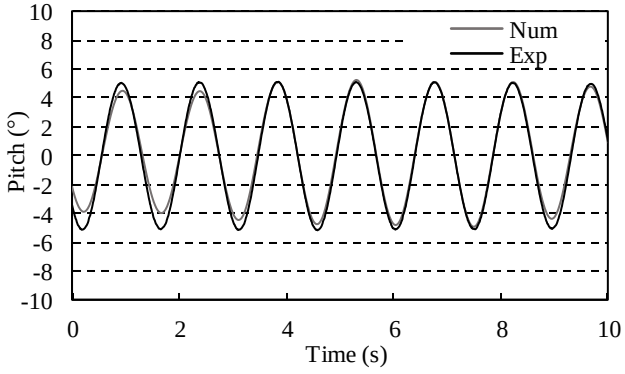

(a)

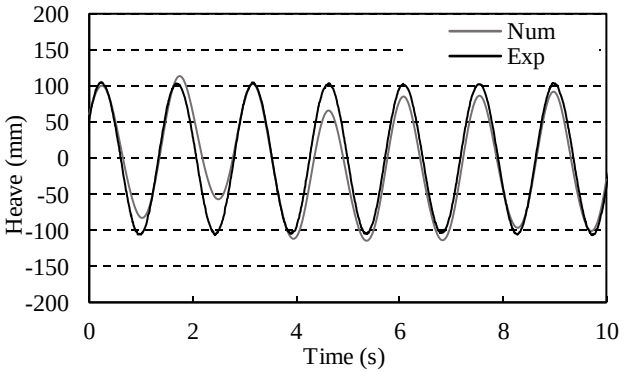

(b)

Figure 18 (a) Pitch measurements for experimental (black) and numerical (grey); and, (b) heave measurements for experimental (black) and numerical (grey) results for test case 8

Fig. 18 shows the results of test case 8. The heave is under predicted at the beginning of the test and pitch is also under predicted at the beginning, however pitch agrees as the test progresses.

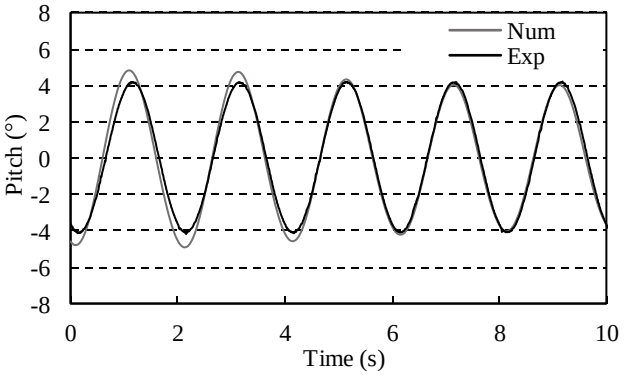

(a)

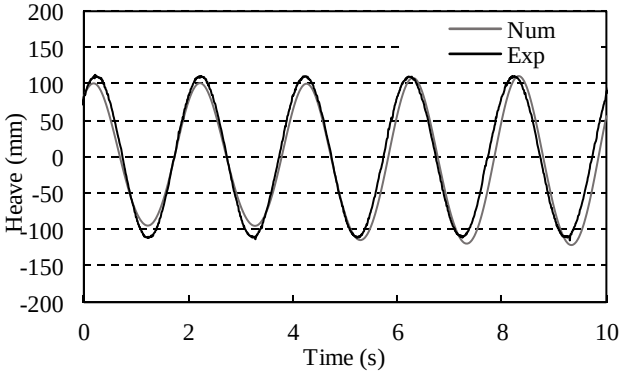

(b)

Figure 19 (a) Pitch measurements for experimental (black) and numerical (grey); and, (b) heave measurements for experimental (black) and numerical (grey) results for test case 9

Fig. 19 shows the results of test case 9. The pitch is over predicted by the numerical model and the heave under predicted.

It was observed that throughout the tests the heave is generally under predicted by the numerical model and the pitch is over predicted. Both of these properties are most likely due to the mooring system being present during the experimental tests whereas the numerical model held the model fixed to represent perfect moorings. In the experimental tests there was a small translation in the direction of wave propagation due to flex in the mooring system allowing the device to respond to the waves.

TABLE III
SHOWING THE HARDWARE USED TO RUN THE TEST CASES AND THE TIME TAKEN FOR EACH CASE

Test Case	CPU	Clock Speed (GHz)	Threads	CPU Time (s)
1	i7-2600	3.4	6	325,550
2	i7-2600	3.4	6	319,635
3	i7-4790k	4.0	6	266,744
4	i7-4790k	4.0	6	268,156
5	i7-4790k	4.0	6	267,977
6	i7-2600	3.4	6	322,887
7	i7-4790k	4.0	6	255,195
8	i7-2600	3.4	6	331,570
9	i7-4790k	4.0	6	265,723

Table III shows the hardware used for the numerical tests and the total time for each run. Higher clock speeds on a newer generation processor resulted in quicker run times. Between tests there is little variation suggesting the runs are similarly computationally demanding.

V. CONCLUSIONS AND FURTHER WORK

Experimental and numerical tests were run on a 1:30 scale model of the WaveCat WEC in the Ocean Basin at the University of Plymouth with the aim of validating a numerical model for regular waves. 6DOF data were gathered from the Qualysis motion capture system during experimental tests with the absence of overtopping on the device. The numerical model was designed in STAR-CCM+ and in general showed good agreement between experimental and numerical results, however the accuracy was less at larger wave heights, particularly in heave.

Typically, the numerical model under predicted pitch and over predicted heave. This is due to the numerical model forcing the model to be fixed in degrees of freedom aside from those monitored. During the experimental tests the model was influenced by wave action in the direction of wave propagation

The results agree with other CFD studies of single hull vessels [24] and multi hull vessels [34] in regular waves in that it shows slight variation between each individual heave and pitch period. This is to be expected as without overtopping the WaveCat is essentially a floating rigid vessel akin to a ship.

It is important to note that this is an ongoing project and as such the model will be refined and additional test cases performed with regular waves and irregular sea states to provide a more comprehensive numerical model. The results presented here are initial steps towards a fully validated numerical model and to setup an appropriate numerical environment for the future objectives.

Future objectives for the project are therefore; (a) to consider a wider range of regular waves; (b) to consider irregular waves and validate with experimental results; (c) to accurately model

moorings as tested in the experimental modelling; (d) to expand the model to include overtopping and potential power generation and validate the model; and (e), to use the validated numerical model as a means of optimising the device.

ACKNOWLEDGMENTS

We are grateful for the funding received by Gregorio Iglesias through a Marie Curie fellowship (WAVEIMPACT, PCIG13-GA-2013-618556).

Additionally, two Santander Seed-corn Scholarships were granted to both James Allen and Jian Wan for the experimental phase of the project and development of the control systems respectively.

The authors would also like to thank the staff of the COAST Laboratory at Plymouth University for their invaluable help in construction and testing the model.

The authors would also like to thank CD-Adapco for the license to use STAR-CCM+ in this project.

REFERENCES

[1] European Parliament Council of the European Union, "Directive 2009/28/EC on the promotion of the use of energy from renewable sources," in *Official Journal of the EU*, ed, 2009, pp. 16-62.

[2] H. Lund, "Renewable energy strategies for sustainable development," *Energy*, vol. 32, pp. 912-919, 2007.

[3] G. Iglesias and R. Carballo, "Wave resource in El Hierro—an island towards energy self-sufficiency," *Renewable Energy*, vol. 36, pp. 689-698, 2011.

[4] G. Iglesias and R. Carballo, "Wave energy resource in the Estaca de Bares area (Spain)," *Renewable Energy*, vol. 35, pp. 1574-1584, 2010.

[5] G. Iglesias and R. Carballo, "Wave energy and nearshore hot spots: The case of the SE Bay of Biscay," *Renewable Energy*, vol. 35, pp. 2490-2500, 2010.

[6] S. P. Neill and M. R. Hashemi, "Wave power variability over the northwest European shelf seas," *Applied Energy*, vol. 106, pp. 31-46, 2013.

[7] R. Guanche, A. De Andrés, I. J. Losada, and C. Vidal, "A global analysis of the operation and maintenance role on the placing of wave energy farms," *Energy Conversion and Management*, vol. 106, pp. 440-456, 2015.

[8] A. López-Ruiz, R. J. Bergillos, and M. Ortega-Sánchez, "The importance of wave climate forecasting on the decision-making process for nearshore wave energy exploitation," *Applied Energy*, vol. 182, pp. 191-203, 2016.

[9] J. Abanades, D. Greaves, and G. Iglesias, "Wave farm impact on the beach profile: A case study," *Coastal Engineering*, vol. 86, pp. 36-44, 2014.

[10] J. Abanades, D. Greaves, and G. Iglesias, "Wave farm impact on beach modal state," *Marine Geology*, vol. 361, pp. 126-135, 2015.

[11] E. Rusu and F. Onea, "Study on the influence of the distance to shore for a wave energy farm operating in the central part of the Portuguese nearshore," *Energy Conversion and Management*, vol. 114, pp. 209-223, 2016.

[12] A. Azzellino, D. Conley, D. Vicinanza, and J. P. Kofoed, "Marine Renewable Energies: Perspectives and Implications for Marine Ecosystems," *The Scientific World Journal*, vol. 2013, p. 3, 2013.

[13] J. Abanades, D. Greaves, and G. Iglesias, "Coastal defence through wave farms," *Coastal Engineering*, vol. 91, pp. 299-307, 2014.

[14] C. Pérez-Collazo, D. Greaves, and G. Iglesias, "A review of combined wave and offshore wind energy," *Renewable and Sustainable Energy Reviews*, vol. 42, pp. 141-153, 2015.

[15] WAMIT. (28/4/17). *Wamit, Inc. - The State of the Art in Wave Interaction Analysis*. Available: http://www.wamit.com/index.htm

[16] ANSYS. (28/4/17). *Fluids - CFD Simulation Software | ANSYS*. Available: http://www.ansys.com/products/fluids

[17] OpenFOAM. (28/4/17). *OpenFOAM® - Official home of The Open Source Computational Fluid Dynamics (CFD) Toolbox*. Available: http://www.openfoam.com/

[18] J. H. Ferziger and M. Peric, *Computational Methods for Fluid Dynamics*: Springer Berlin Heidelberg, 2012.

[19] H. Fernandez, G. Iglesias, R. Carballo, A. Castro, J. A. Fraguela, F. Taveira-Pinto, *et al.*, "The new wave energy converter WaveCat: Concept and laboratory tests," *Marine Structures*, vol. 29, pp. 58-70, 2012.

[20] H. Fernandez, G. Iglesias, R. Carballo, A. Castro, M. Sanchez, and F. Taveira-Pinto, "Optimization of the WaveCat Wave Energy Converter," *Coastal Engineering*, 2012.

[21] G. Iglesias, H. Fernandez, R. Carballo, A. Castro, and F. Taveira-Pinto, "The WaveCat© - Development of a new Wave Energy Converter," presented at the World Renewable Energy Congress, Linkoping, Sweden, 2011.

[22] J. Allen, K. Sampanis, J. Wan, D. Greaves, J. Miles, and G. Iglesias, "Laboratory Tests in the Development of WaveCat," *Sustainability*, vol. 8, 2016.

[23] Y. H. Ozdemir and B. Barlas, "Numerical study of ship motions and added resistance in regular incident waves of KVLCC2 model," *International Journal of Naval Architecture and Ocean Engineering*, vol. 9, pp. 149-159, 2017.

[24] T. Tezdogan, A. Incecik, and O. Turan, "Full-scale unsteady RANS simulations of vertical ship motions in shallow water," *Ocean Engineering*, vol. 123, pp. 131-145, 2016.

[25] S. P. Kim, "CFD as a seakeeping tool for ship design," *International Journal of Naval Architecture and Ocean Engineering*, vol. 3, pp. 65-71, 2011.

[26] Y.-H. Yu and Y. Li, "Reynolds-Averaged Navier–Stokes simulation of the heave performance of a two-body floating-point absorber wave energy system," *Computers & Fluids*, vol. 73, pp. 104-114, 2013.

[27] A. Elhanafi, A. Fleming, G. Macfarlane, and Z. Leong, "Numerical hydrodynamic analysis of an offshore stationary–floating oscillating water column–wave energy converter using CFD," *International Journal of Naval Architecture and Ocean Engineering*, vol. 9, pp. 77-99, 2017.

[28] M. Bozorgnia, A. Eftekharian, and J. J. Lee, "CFD MODELING OF A SOLITARY WAVE OVERTOPPING BREAKWATER OF VARYING SUBMERGENCE," *Coastal Engineering Proceedings; No 34 (2014)*, 2014.

[29] S. Jungrungruengtaworn and B.-S. Hyun, "Influence of slot width on the performance of multi-stage overtopping wave energy converters," *International Journal of Naval Architecture and Ocean Engineering*, 2017.

[30] CD-Adapco, *STAR-CCM+ User Guide 12.02*, 2017.

[31] E. Schreck, M. Peric, and D. Snyder. (2012, 08/07/17). *Overset grids technology in STAR-CCM+: Methodology and applications*. Available: http://2012.oversetgridsymposium.org/assets/pdf/presentations/2_3/Overset_Schreck_Peric_Snyder.pdf

[32] C. W. Hirt and B. D. Nichols, "Volume of fluid (VOF) method for the dynamics of free boundaries," *Journal of Computational Physics*, vol. 39, pp. 201-225, 1981.

[33] J. Choi and S. B. Yoon, "Numerical simulations using momentum source wave-maker applied to RANS equation model," *Coastal Engineering*, vol. 56, pp. 1043-1060, 2009.

[34] C. Wu, D. Zhou, L. Gao, and Q. Miao, "CFD computation of ship motions and added resistance for a high speed trimaran in regular head waves," *International Journal of Naval Architecture and Ocean Engineering*, vol. 3, pp. 105-110, 2011.